



OPEN

Controllable large positive and negative Goos–Hänchen shifts with a double-Lambda atomic system

Anas Othman¹, Saeed Asiri²✉ & M. Al-Amri^{2,3}

We study the Goos–Hänchen shift (GHS) of a reflected light beam from a cavity containing a double- Λ atomic medium that is bounded by two glass slabs. Applying both coherent and incoherent fields to the atomic medium leads to positive and negative controllability of GHS. For some specific values of the parameters of the system, the amplitude of the GHS becomes large, namely, in the order of $\sim 10^3$ times the wavelength of the incident light beam. These large shifts are found at more than one angle of incidence with a wide range of parameters of the atomic medium.

Goos–Hänchen shift (GHS) is a phenomena, which occurs when a light beam is incident on a medium with a refractive index smaller than that of the medium of incidence. For an angle of incidence greater than the critical angle, the incident beam penetrates for some distance inside the second medium^{1–6} and reflects back to the first (incident) medium, in which the reflected beam is laterally shifted at the interface from the point at which the incident beam entered the second medium. This lateral displacement is named Goos–Hänchen shift after its experimental demonstration in 1947 by Goos and Hänchen^{7,8}. Several theoretical proposals have been suggested to calculate the GHS such as the stationary phase method, which was developed by Artmann⁹. Another method based on the concept of energy conservation was introduced by Renard to theoretically calculate the GHS¹⁰.

Many structures and designs with different materials have been proposed to measure and control the GHS. For example, studying GHS in low absorbing media^{11–13} and in epsilon-near-zero slab^{14,15}. Also, in different arrangements of defective and normal photonic crystals^{16–18}. Further examples of the investigation of GHS include using two layers of different artificial media^{19–21}, a cavity containing colloidal ferrofluids²² and graphene layers^{23,24} are all reported. More recently, GHS with an amplitude reaching four times of the wavelength of the incident light is obtained in a structure containing a periodic grating layer^{25,26}. In addition to all of the previous examples, GHS was also observed experimentally for a transmitted beam in one-dimensional photonic crystal slabs²⁷.

On the other hand, various atomic media where the optical properties of these media can be modified by some external parameters such as coherent fields were proposed and applied for different purposes^{28–33}. The use of such atomic media to manipulate and control the GHS^{34–38} has been suggested. In³⁴, a driven two-level system is used in a three layers cavity to coherently control the GHS. In^{37,39}, the GHS is studied using the same cavity structure and containing a Λ atomic scheme, where positive and negative lateral shifts were reported. Moreover, different four-level atomic structures^{40–42} including the double- Λ atomic system^{43,44} are studied along with different techniques.

In this report, we show that the double- Λ atomic system, which has two probe interactions can be used to produce large GHS in the order of $10^3\lambda$. The double- Λ scheme has relatively large controllable dispersion feature greater than the Λ atomic scheme with limited absorption⁴⁵. This great controllability makes the double- Λ scheme an excellent candidate to produce very large GHS. Therefore, we study the effect of different parameters on the GHS in a cavity containing three layers where the middle layer is filled by the double- Λ atoms.

Results

Model. We consider a TE-polarized light field with a frequency ω_p is incident from vacuum with an angle θ on a cavity consisting of three layers of nonmagnetic materials. The first and last layers are identical and have a thickness d_1 , while the middle layer has a thickness d_2 as shown in Fig. 1a. The electric permittivity of the edge

¹Department of Physics, Faculty of Science, Taibah University, Al Madinah Al Munawwarah, Saudi Arabia. ²Institute of Quantum Technologies and Advanced Computing, KACST, Riyadh 11442, Saudi Arabia. ³NCQOQI, KACST, Riyadh 11442, Saudi Arabia. ✉email: sasiri@kacst.edu.sa

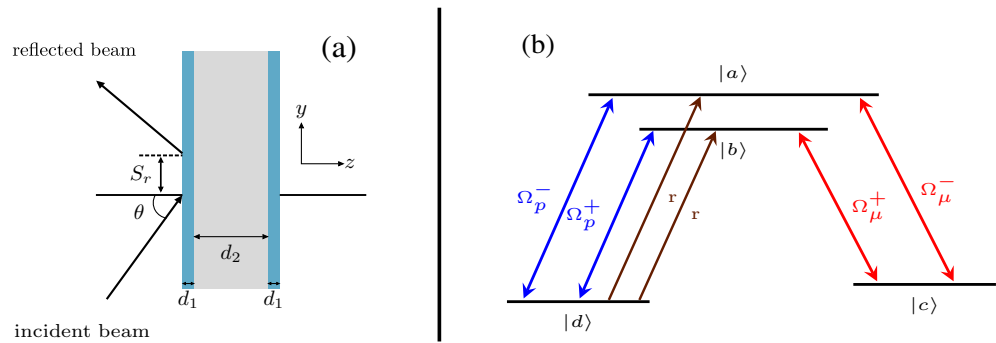


Figure 1. (a) Configuration of the three layers cavity, which consists of two glass slabs having the same thickness d_1 surrounding an intracavity of thickness d_2 . A light beam is incident on the cavity with an angle of incidence θ and the reflected beam is laterally shifted on the y -axis. This lateral shift S_r is known as the Goos–Hänchen Shift (GHS). (b) The double- Λ atomic scheme, which is placed in the intracavity to control the GHS.

and intracavity layers are ϵ_1 and ϵ_2 , respectively. The double- Λ atomic medium is placed in the second layer. The atomic system as shown in Fig. 1b has four levels ($|a\rangle$, $|b\rangle$, $|c\rangle$, and $|d\rangle$) where the transitions $|a\rangle \leftrightarrow |d\rangle$ and $|b\rangle \leftrightarrow |c\rangle$ are coupled by two probe fields with Rabi frequencies Ω_p^- and Ω_p^+ , respectively. Two strong coherent fields are driving the transitions $|a\rangle \leftrightarrow |c\rangle$ and $|b\rangle \leftrightarrow |d\rangle$ with Rabi frequencies Ω_μ^- and Ω_μ^+ , respectively. Also, the system is pumped by two incoherent fields from the state $|d\rangle$ to $|a\rangle$ and $|b\rangle$ with the same rate r . The double- Λ system exists for example in rubidium and sodium^{46,47}. We choose the D_2 transition in ^{85}Rb where the states $|a\rangle$ and $|b\rangle$ correspond to the hyperfine levels with $F = 4$, $m_F = 0$ and $F = 3$, $m_F = 0$, respectively. The lower levels $|c\rangle$ and $|d\rangle$ correspond to the hyperfine level $F = 3$ with magnetic sublevels $m_F = +1$ and $m_F = -1$, respectively. Therefore, right and left circularly polarized fields (σ^\pm) are used for both the probe and driving fields. All different fields are assumed to be homogeneous through the whole cavity.

The Hamiltonian of the double- Λ atomic system⁴⁵ in the dipole and rotating wave approximations is written as

$$H = \hbar \left[\omega_a |a\rangle \langle a| + \omega_b |b\rangle \langle b| + \omega_c |c\rangle \langle c| + \omega_d |d\rangle \langle d| - \frac{\Omega_p^-}{2} e^{i\Delta_1 t} |a\rangle \langle d| - \frac{\Omega_p^+}{2} e^{i\Delta_2 t} |b\rangle \langle d| - \frac{\Omega_\mu^+}{2} e^{i\Delta_3 t} |b\rangle \langle c| - \frac{\Omega_\mu^-}{2} e^{i\Delta_4 t} |a\rangle \langle c| + H.c. \right], \quad (1)$$

where ω_a , ω_b , ω_c , and ω_d are the frequencies of the energy levels $|a\rangle$, $|b\rangle$, $|c\rangle$, and $|d\rangle$, respectively. The Rabi frequencies of the two probe fields are Ω_p^- and Ω_p^+ , whereas the Rabi frequencies of the driving fields are Ω_μ^- and Ω_μ^+ . The detunings in Eq. (1) are defined such that $\Delta_1 = \omega_{ad} - \omega_p$, $\Delta_2 = \omega_{bd} - \omega_p$, $\Delta_3 = \omega_{bc} - \omega_\mu$, and $\Delta_4 = \omega_{ac} - \omega_\mu$, where we assumed that the two probe fields have the same frequency ω_p , and the two driving fields have the same frequency ω_μ . The equations of motion for the density matrix elements can be derived using the master equation^{45,48} along with the Hamiltonian Eq. (1). These equations of motion can be solved to the first order at steady state when considering weak probe of the system. The permittivity of the middle layer ϵ_2 is defined in terms of the susceptibility of the atomic system as $\epsilon_2 = 1 + \chi$. The dielectric susceptibility of the system⁴⁵ has two parts χ_{ad} and χ_{bd} , which come from the double probe interactions with the atomic medium. Therefore, the susceptibility is expressed as $\chi = \chi_{ad} + \chi_{bd}$ in which these two parts are given by

$$\chi_{bd} = \frac{i}{D_{bd} + \frac{|\Omega_\mu^+|^2}{4D_{cd}}} \left[\mathcal{C} \left(\frac{|\Omega_\mu^+|^2}{4D_{cd}D_{bc}^*} P_{bc} - P_{bd} \right) - \mathcal{B} \left(\frac{\Omega_\mu^+ \Omega_\mu^{*-}}{4D_{cd}D_{ac}^*} P_{ca} \right) \right], \quad (2)$$

and

$$\chi_{ad} = \frac{i}{D_{ad} + \frac{|\Omega_\mu^-|^2}{4D_{cd}}} \left[\mathcal{B} \left(\frac{\Omega_\mu^- \Omega_\mu^{+*}}{4D_{cd}D_{bc}^*} P_{bc} \right) - \mathcal{A} \left(\frac{|\Omega_\mu^-|^2}{4D_{cd}D_{ac}^*} P_{ca} + P_{ad} \right) \right], \quad (3)$$

where $D_{bd} = \gamma_{bd} - i(\Delta + \omega_{ab}/2)$, $D_{ad} = \gamma_{ad} - i(\Delta - \omega_{ab}/2)$, $D_{cd} = \gamma_{cd} - i(\Delta_\mu + \Delta)$, $D_{bc} = \gamma_{bc} + i(\Delta_\mu - \omega_{ab}/2)$ and $D_{ac} = \gamma_{ac} + i(\Delta_\mu + \omega_{ab}/2)$.

The parameter $P_{ij} = \rho_{ii}^{(0)} - \rho_{jj}^{(0)}$, is the population difference between the states $|i\rangle$ and $|j\rangle$ where $i, j \in (a, b, c, d)$. The expressions of these populations are given as⁴⁵

$$\rho_{aa}^{(0)} = r \frac{R_a(\gamma_b + \gamma_B) + \gamma_B R_a + \gamma_b R_b + 2R_a R_b}{a_1 R_a + a_2 R_b + a_3 R_a R_b + a_4}, \quad (4a)$$

$$\rho_{bb}^{(0)} = r \frac{R_b(\gamma_a + \gamma_A) + \gamma_a R_a + \gamma_A R_b + 2R_a R_b}{a_1 R_a + a_2 R_b + a_3 R_a R_b + a_4}, \quad (4b)$$

$$\rho_{dd}^{(0)} = \frac{\gamma_a \rho_{aa} + \gamma_b \rho_{bb}}{2r}, \quad (4c)$$

$$\rho_{cc}^{(0)} = 1 - \rho_{aa}^{(0)} - \rho_{bb}^{(0)} - \rho_{cc}^{(0)}. \quad (4d)$$

The detailed expressions of the rest the parameters a_1, a_2, a_3, a_4, R_a , and R_b can be found in⁴⁵. The decay rates are denoted by γ_i , and $\gamma_{ij} = (\gamma_i + \gamma_j)/2$, is the average of the decay rates of the states $|i\rangle$ and $|j\rangle$. The values of the decay rates are $\gamma_a = \gamma_b = 0.7\gamma$, $\gamma_A = \gamma_B = 0.2\gamma$, $\gamma_{ab} = \gamma_{cd} = 0$, and $\gamma_{ac} = \gamma_{bc} = \gamma_{ad} = \gamma_{bd} = (\gamma_a + \gamma_A)/2 = 0.5\gamma$, where $\gamma = 10$ MHz. The parameters Δ and Δ_μ are defined as $\Delta = \omega_p - W_p$ and $\Delta_\mu = W_\mu - \omega_\mu$, where $W_p = (\omega_{ad} + \omega_{bd})/2$, $W_\mu = (\omega_{ac} + \omega_{bc})/2$, and $\omega_{ij} = \omega_i - \omega_j$ is the energy difference between the two states $|i\rangle$ and $|j\rangle$. $\mathcal{A}, \mathcal{B}, \mathcal{C}$ are the density parameters. Also, $\Omega_\mu^+ = \Omega_\mu^-/\alpha$, where α is the ratio between the two driving fields.

The GH shift. The GHS of the reflected TE-polarized light field S_r can be calculated using the result of the stationary phase theory⁹, which is given by

$$S_r = -\frac{d\phi_r}{dk_y}, \quad (5)$$

where $k_y = k \sin \theta$ is the parallel component of the wavevector, $k = \omega_p/c$ where c is the speed of light in vacuum. The function ϕ_r represents the phase shift, which corresponds to the reflected field. The phase shift of the reflected TE-polarized field is directly related to the reflection coefficient r^{TE} via $\phi_r = \tan^{-1} [\text{Im}(r^{\text{TE}})/\text{Re}(r^{\text{TE}})]$.

We calculate the reflection coefficient r^{TE} of the three layers cavity for the TE-polarized field using the standard characteristic matrix approach^{49,50}, which enables connecting the field through the layers of the cavity. Following the same approach as, for example in^{34,37}, the reflection coefficient for the TE-polarized field r^{TE} is given as

$$r^{\text{TE}}(\theta, \omega_p) = \frac{\cos \theta (X_{22}^{\text{TE}} - X_{11}^{\text{TE}}) - (\cos^2 \theta X_{12}^{\text{TE}} - X_{21}^{\text{TE}})}{\cos \theta (X_{22}^{\text{TE}} + X_{11}^{\text{TE}}) - (\cos^2 \theta X_{12}^{\text{TE}} + X_{21}^{\text{TE}})}, \quad (6)$$

where X_{ij}^{TE} is the matrix element of the total transfer matrix of the three layers cavity. The total transfer matrix for our configuration is given by

$$X^{\text{TE}}(\theta, \omega_p) = M_1^{\text{TE}}(\theta, \omega_p, d_1) M_2^{\text{TE}}(\theta, \omega_p, d_2) M_1^{\text{TE}}(\theta, \omega_p, d_1). \quad (7)$$

For any single layer, the transfer matrix can be calculated from

$$M_j^{\text{TE}}(\theta, \omega_p, d_j) = \begin{pmatrix} \cos[n_j k \cos(\theta_j) d_j] & i \sin[n_j k \cos(\theta_j) d_j] / (n_j \cos(\theta_j)) \\ i n_j \cos(\theta_j) \sin[n_j k \cos(\theta_j) d_j] & \cos[n_j k \cos(\theta_j) d_j] \end{pmatrix}, \quad (8)$$

where $\sin \theta_j = \sin \theta / n_j$, $k = \omega_p/c$ is the wave number of the incident probe field in vacuum with probe frequency ω_p , while n_j is the refractive index of the j -th layer in the cavity, and d_j is the thickness of the j th layer.

The parameters in our configuration can be selected to be similar to most of the articles applying the same three layers cavity. The thickness of the layers are $d_1 = 0.2 \mu\text{m}$, $d_2 = 5 \mu\text{m}$, and the permittivity of the edge layers is $\epsilon_1 = 2.22$. Next, the parameters of the double- Λ atomic medium are⁴⁵ as follows: $\omega_{ab} = 12.1\gamma$, $W = 2\pi \times 300$ THz, $\Delta = -5\gamma$, $\Delta_\mu = 0$, $\mathcal{A} = 1.1\gamma$, $\mathcal{B} = 1.05\gamma$, and $\mathcal{C} = \gamma$, where $\gamma = 10$ MHz. The free parameters, which will be studied are Ω_μ , r , and θ , where $\Omega_\mu^- = \Omega_\mu^+ = \Omega_\mu$ and $\alpha = 1$.

Next, we proceed with the calculations of the GHS. To have a glance over the capability of our system to control the GHS, we plot the GHS of the reflected beam versus the angle of incidence θ from 0 to $\pi/2$ for some selected parameters of the atomic medium. We see in Fig. 2 that both the amplitude and direction of the GHS can be changed when changing r . Needless to mention that our system is tuned and controlled remotely by simply manipulating the values of the pump r and Rabi frequency of the driving fields Ω_μ yielding a significant change in the behavior of the GHS, while the cavity structure is kept intact.

In the following, we study the dependence of the lateral shift of the reflected beam on the external parameters r and Ω_μ . Our purpose is to see the behavior of the GHS by only changing the parameters of the atomic medium, namely r and Ω_μ , and without changing the structure of the cavity. We also can find out which values of r and Ω_μ can produce large GHS.

The effect of r . We study the effect of the pumping rate r on the GHS while the driving fields are fixed. In Fig. 3, we plot the GHS of the reflected light beam S_r versus r for different values of Ω_μ , while the angle of incidence is assumed to be $\theta = 62^\circ$. The GHS in Fig. 3 can be positive or negative for the selected values of Ω_μ . In Fig. 3a, it is noticed that around some specific values of the pumping rate r , the GHS is large in comparison to the wavelength of the incident light beam, i.e., in the order of $10^2 \lambda$ when $\Omega_\mu = 5\gamma$. When $\Omega_\mu = 7\gamma$, large positive GHS in the order of nearly $10^3 \lambda$ occurs at $r \approx 3\gamma$ as seen in Fig. 3b.

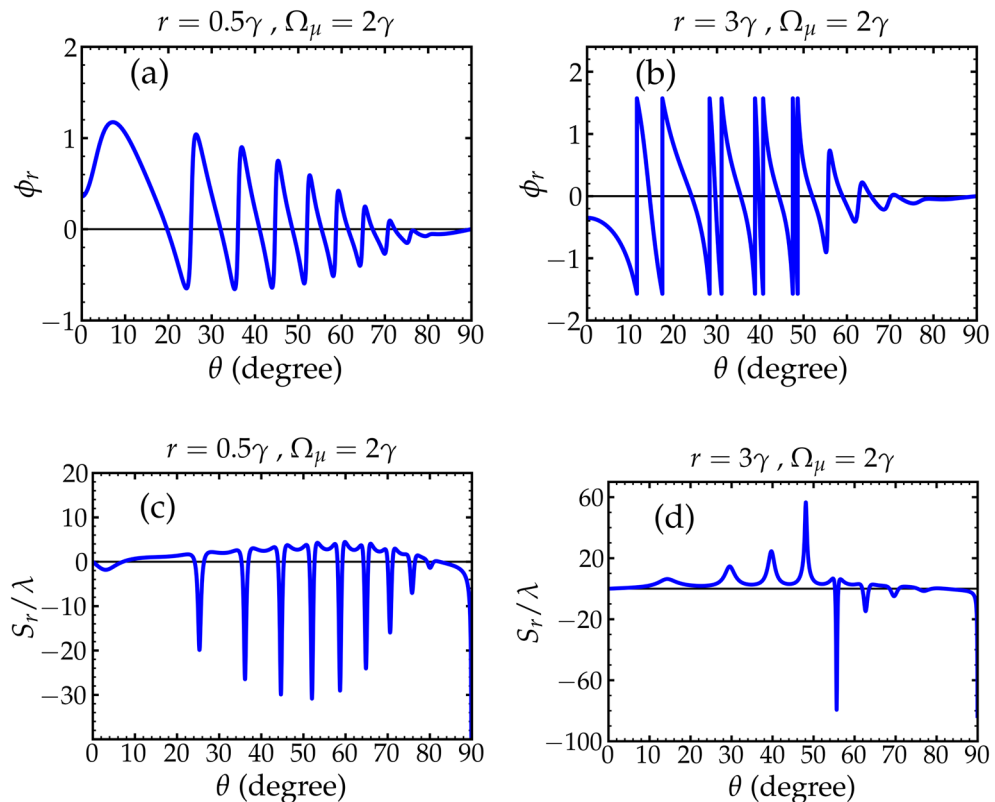


Figure 2. (a) and (b) shows the relative phase of the reflected beam versus the angle of incidence θ . (c) and (d) shows the dependence of the GHS of the reflected light beam on the angle of incidence θ . The pumping rate values are $r = 0.5\gamma$ in (a) and (c), while $r = 3\gamma$ in (b) and (d). The driving field $\Omega_\mu = 2\gamma$ in (a)–(d). The amplitude of the GHS becomes large at angles of incidence where sharp phase changes occur. Other parameters are shown in the text.

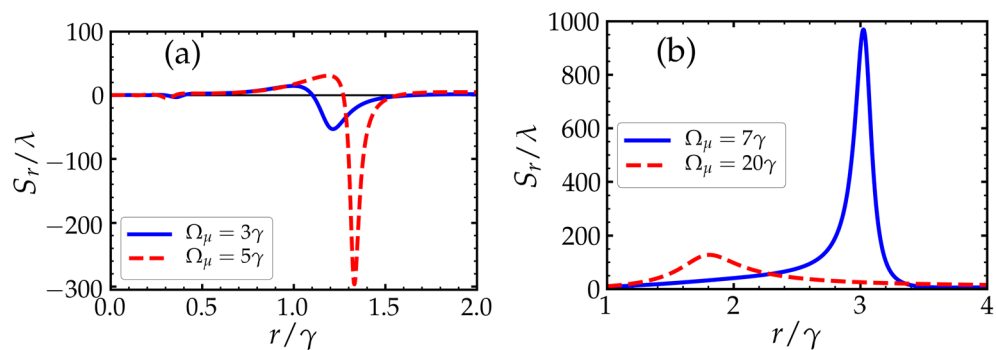


Figure 3. The GHS of the reflected light field S_r versus the pumping rate r for different values of driving fields Ω_μ . The driving field values in (a) are $\Omega_\mu = 3\gamma$ (solid) and $\Omega_\mu = 5\gamma$ (dashed). Similarly, $\Omega_\mu = 7\gamma$ (solid) and $\Omega_\mu = 20\gamma$ (dashed) in (b). Other parameters are shown in the text.

The effect of Ω_μ . In this subsection, we explore the dependence of the GHS of the reflected beam on the Rabi frequency of the driving fields Ω_μ . From the previous study (Sec. III. A), we obtained large GHS at certain values of r . Figure 4 shows the dependence of the GHS on Ω_μ , where large negative and positive GHS occur over some range of Ω_μ .

In Fig. 4a, we plot the GHS with Ω_μ for two different values of r . We observe large positive shifts in the order of $10^2\lambda$ over a relatively wide range of Ω_μ . This indicates it is flexible to choose the value of Ω_μ that produces a large positive GHS in this situation.

In Fig. 4b, we see that large shifts are achieved at different points of Ω_μ as r is modified. For example, when $r = 3\gamma$, we observe a large positive GHS, i.e., $S_r \approx -10^3\lambda$ at $\Omega_\mu \approx 7\gamma$. In fact, these large shifts are continuous

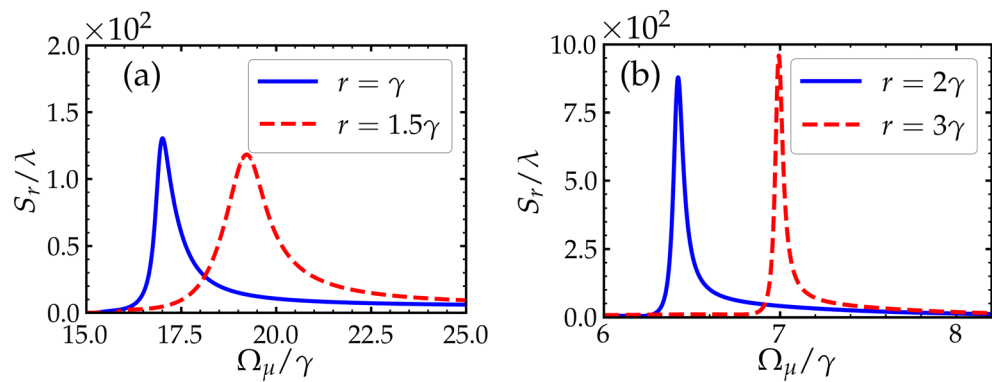


Figure 4. The dependence of the GHS on the driving fields Ω_μ for different values of pumping rates r . Other parameters are shown in the text.

in the selected range of the values of r . Therefore, this suggests that we can pick a pair (r, Ω_μ) that produces large shifts in the orders of $10^3 \lambda$.

Other angles. So far, the analysis of the GHS have been carried out when the angle of incidence is $\theta = 62^\circ$. It should be pointed out that not all angles under our selected parameters can necessarily produce large shifts. Here, we show that large positive or negative GHS at other selected values of the angle of incidence can still be observed.

In Fig. 5, we see that the GHS of the reflected beam reaches values of order $10^3 \lambda$ under specific values of the pair (r, Ω_μ) . In all the reported results for the selected angles here, we observe large positive and negative GHS as the value of r is modified. For example, in Fig. 5a where the angle of incidence is $\theta = 56^\circ$, the GHS is reaching an order of $10^3 \lambda$, which is relatively large shift where that occurs at a wide range of Ω_μ . Similarly in Fig. 5b where the angle of incidence is assumed to be $\theta = 65^\circ$, large positive and negative GHS are observed for some specific values of r for a small range of Ω_μ . Thus, for each angle, to find a large GHS, one needs to perform some kind of an optimization in order to find the suitable value of the pair (r, Ω_μ) at which a large shift can occur.

Incident Gaussian beam. All the previous results of the GHS are obtained using the expression derived by Artmann Eq. (5)^{6,9}. Artmann derived this result to calculate the GHS assuming that the incident beam is a plane wave. When measuring the GHS experimentally, one would usually consider a laser beam, which has a Gaussian profile. As shown in³⁴, we examine the validity of Artmann's expression considering that the incident light in our system is a Gaussian beam, which can be written as

$$E_x^i(y, z = 0) = \frac{1}{\sqrt{2\pi}} \int B(k_y) e^{ik_y y} dk_y. \quad (9)$$

Similarly, the reflected light beam at the interface is given by

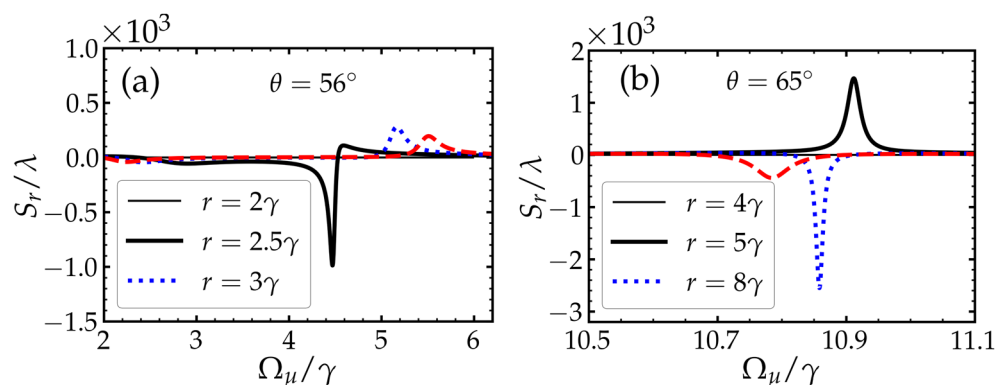


Figure 5. The GHS of the reflected beam against the driving field Ω_μ for different values of the pumping rate r . The angles of incidence in (a) and (b) are $\theta = 56^\circ$ and $\theta = 65^\circ$, respectively. Other parameters are shown in the text.

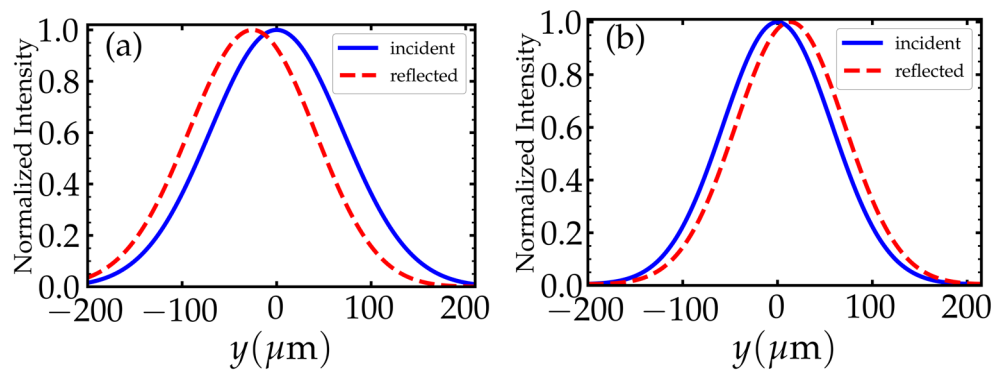


Figure 6. The normalized intensity distribution of the incident (solid) and reflected (dashed) light beams with $W = 100\lambda$. The angle of incidence in (a) is $\theta = 44.6^\circ$ with $r = 0.5\gamma$ and $\Omega_\mu = 2\gamma$. In (b), $\theta = 30^\circ$ with $r = 3\gamma$ and $\Omega_\mu = 2\gamma$. Other parameters are shown in the text.

$$E_x^r(y, z = 0) = \frac{1}{\sqrt{2\pi}} \int r^{\text{TE}}(k_y, \omega_p) B(k_y) e^{ik_y y} dk_y. \quad (10)$$

Here $B(k_y)$ is the angular spectrum distribution of the Gaussian beam, which is given by

$$B(k_y) = \frac{W_y}{\sqrt{2}} \exp\left[-\frac{W_y^2(k_y - k_{y0})^2}{4}\right], \quad (11)$$

with $W_y = W/\cos\theta$ and $k_{y0} = k\sin\theta$, where W represents the half width of the Gaussian beam at the interface. The position of the maximum normalized intensity distribution of the incident and reflected beams at the interface ($z = 0$) can be calculated by

$$\langle y^{i/r} \rangle = \frac{\int y |E_x^{i/r}(y, z = 0)|^2 dy}{\int |E_x^{i/r}(y, z = 0)|^2 dy}, \quad (12)$$

where the superscripts i and r indicate the incident and reflected beams, respectively. The GHS in this situation is given by the difference between the positions of the maximum points of the intensity profile of the incident and reflected beams, i.e., $\langle y^r \rangle - \langle y^i \rangle$. We choose $W = 100\lambda$ in the calculations of the GHS using Eq. (12). In Fig. 6a, $\langle y^r \rangle - \langle y^i \rangle \approx -28 \mu\text{m}$ and in Fig. 6b $\langle y^r \rangle - \langle y^i \rangle \approx 13 \mu\text{m}$. These results of the lateral shift agree with the results, which are calculated using the stationary phase approach shown in Figs. 2a, 3b, respectively. Hence, this method confirms the validity of Artmann's formula Eq. (5) of the GHS.

Discussion

We investigated the control of the GHS of the reflected light beam using a double- Λ atomic medium placed inside a cavity bounded by two glass slabs. We showed that the GHS of the reflected beam can be controlled remotely by simply changing the values of the pump r and Rabi frequency of the driving fields Ω_μ , while the cavity structure is kept intact. We also found that our system is capable of producing very large GHS of orders $10^3\lambda$ at more than one angle of incidence.

Data availability

The datasets that support the plots in this paper are available from the corresponding author on reasonable request.

Received: 22 December 2022; Accepted: 27 February 2023

Published online: 07 March 2023

References

1. Lotsch, H. K. V. Reflection and refraction of a beam of light at a plane interface. *J. Opt. Soc. Am.* **58**, 551 (1968).
2. Lotsch, H. K. V. Reflection and refraction of a beam of light at a plane interface. *Optik (Jena)* **32**, 116 (1970).
3. Lotsch, H. K. V. Reflection and refraction of a beam of light at a plane interface. *Optik (Jena)* **32**, 189 (1970).
4. Lotsch, H. K. V. Reflection and refraction of a beam of light at a plane interface. *Optik (Jena)* **32**, 299 (1971).
5. Lotsch, H. K. V. Reflection and refraction of a beam of light at a plane interface. *Optik (Jena)* **32**, 553 (1971).
6. Li, C.-F. Negative lateral shift of a light beam transmitted through a dielectric slab and interaction of boundary effects. *Phys. Rev. Lett.* **91**, 133903 (2003).
7. Goos, F. & Hänchen, H. Ein neuer und fundamentaler Versuch zur Totalreflexion. *Ann. Phys.* **1**, 333 (1947).
8. Goos, F. & Hänchen, H. Neumessung des Strahlversetzungseffektes bei Totalreflexion. *Ann. Phys.* **5**, 251 (1949).
9. Artmann, K. Berechnung der Seitenversetzung des totalreflektierten Strahles. *Ann. Phys.* **2**, 87 (1948).
10. Renard, R. H. Total reflection: A new evaluation of the Goos–Hänchen shift. *J. Opt. Soc. Am.* **54**, 1190 (1964).

11. Lai, H. M. & Chan, S. W. Large and negative Goos–Hänchen shift near the Brewster dip on reflection from weakly absorbing media. *Opt. Lett.* **27**, 680 (2002).
12. Wang, L.-G., Chen, H. & Zhu, S.-Y. Large negative Goos–Hänchen shift from a weakly absorbing dielectric slab. *Opt. Lett.* **30**, 2936 (2005).
13. Wang, L.-G. & Zhu, S.-Y. Large positive and negative Goos–Hänchen shifts from a weakly absorbing left-handed slab. *J. Appl. Phys.* **98**, 043522 (2005).
14. Xu, Y., Chan, C. T. & Chen, H. Goos–Hänchen effect in epsilon-near-zero metamaterials. *Sci. Rep.* **5**, 8681 (2015).
15. Wen, J., Zhang, J., Wang, L.-G. & Zhu, S.-Y. Goos–Hänchen shifts in an epsilon-near-zero slab. *J. Opt. Soc. Am. B.* **34**, 2310 (2017).
16. Felbacq, D., Moreau, A. & Smaïli, R. Goos–Hänchen effect in the gaps of photonic crystals. *Opt. Lett.* **28**, 1633 (2003).
17. Soboleva, I. V., Moskalenko, V. V. & Fedyanin, A. A. Giant Goos–Hänchen effect and fano resonance at photonic crystal surfaces. *Phys. Rev. Lett.* **108**, 123901 (2012).
18. Wang, L. G. & Zhu, S.-Y. Giant lateral shift of a light beam at the defect mode in one-dimensional photonic crystals. *Opt. Lett.* **31**, 101 (2006).
19. Berman, P. R. Goos–Hänchen shift in negatively refractive media. *Phys. Rev. E* **66**, 067603 (2002).
20. Lakhtakia, A. On planewave remittances and Goos–Hänchen shifts of planar slabs with negative real permittivity and permeability. *Electromagnetics* **23**, 71 (2003).
21. Qing, D.-K. & Chen, G. Goos–Hänchen shifts at the interfaces between left- and right-handed media. *Opt. Lett.* **29**, 872 (2004).
22. Luo, C., Dai, X., Xiang, Y. & Wen, S. Enhanced and tunable Goos–Hänchen shift in a cavity containing colloidal ferrofluids. *IEEE Photon. J.* **7**, 6100310 (2015).
23. Zhang, Q. & Chan, K. S. A spin beam splitter in graphene through the Goos–Hänchen shift. *Appl. Phys. Lett.* **105**, 212408 (2014).
24. Wu, Z., Zhai, F., Peeters, F. M., Xu, Q. H. & Chang, K. Valley-dependent brewster angles and Goos–Hänchen effect in strained graphene. *Phys. Rev. Lett.* **106**, 176802 (2014).
25. Wu, F. *et al.* Giant enhancement of the Goos–Hänchen shift assisted by quasibound states in the continuum. *Phys. Rev. Appl.* **12**, 014028 (2019).
26. Wu, F. *et al.* Dual quasibound states in the continuum in compound grating waveguide structures for large positive and negative Goos–Hänchen shifts with perfect reflection. *Phys. Rev. A* **104**, 023518 (2021).
27. Du, S. *et al.* Realization of large transmitted optical Goos–Hänchen shifts in photonic crystal slabs. *Nanophotonics* **11**, 4531 (2022).
28. Scully, M. O. Enhancement of the index of refraction via quantum coherence. *Phys. Rev. Lett.* **67**, 1855 (1991).
29. Thommen, Q. & Mandel, P. Electromagnetically induced left handedness in optically excited four-level atomic media. *Phys. Rev. Lett.* **96**, 053601 (2006).
30. Zhang, J.-X., Zhou, H.-T., Wang, D.-W. & Zhu, S.-Y. Enhanced reflection via phase compensation from anomalous dispersion in atomic vapor. *Phys. Rev. A* **83**, 053841 (2011).
31. Zhou, H.-T., Wang, D.-W., Wang, D., Zhang, J.-X. & Zhu, S.-Y. Efficient reflection via four-wave mixing in a Doppler-free electromagnetically-induced-transparency gas system. *Phys. Rev. A* **84**, 053835 (2011).
32. Yafan, D., Gongwei, L., Shicheng, Z., Yueping, N. & Shangqing, G. Low light level all-optical switching in a four-level atom-cavity system. *Opt. Commun.* **358**, 73 (2016).
33. Othman, A. A. & Yevick, D. Enhanced negative refractive index control in a 5-level system. *J. Mod. Opt.* **64**, 1208 (2017).
34. Wang, L.-G., Ikram, M. & Zubairy, M. S. Control of the Goos–Hänchen shift of a light beam via a coherent driving field. *Phys. Rev. A* **77**, 023811 (2008).
35. Ziauddin, Q. S. & Zubairy, M. S. Coherent control of the Goos–Hänchen shift. *Phys. Rev. A* **81**, 023821 (2010).
36. Hamed, H. R., Radmehr, A. & Sahrai, M. Manipulation of Goos–Hänchen shifts in the atomic configuration of mercury via interacting dark-state resonance. *Phys. Rev. A* **90**, 053836 (2014).
37. Asiri, S., Xu, J., Al-Amri, M. & Zubairy, M. S. Controlling the Goos–Hänchen and Imbert–Fedorov shifts via pump and driving fields. *Phys. Rev. A* **93**, 013821 (2016).
38. Wan, R.-G. & Zubairy, M. S. Coherent control of spatial and angular Goos–Hänchen shifts in a metal-clad waveguide structure. *Phys. Rev. A* **101**, 023837 (2020).
39. Zhang, X.-J. *et al.* Controlling transverse shift of the reflected light via high refractive index with zero absorption. *Opt. Express* **25**, 10335 (2017).
40. Ziauddin Lee, R.-K. & Qamar, S. Goos–Hänchen shifts of partially coherent light beams from a cavity with a four-level Raman gain medium. *Opt. Commun.* **374**, 45 (2016).
41. Asadpour, S. H., Hamed, H. R. & Jafari, M. Enhancement of Goos–Hänchen shift due to a Rydberg state. *Appl. Opt.* **57**, 4013 (2018).
42. Jafarzadeh, H. & Payravi, M. Theoretical investigation of tunable Goos–Hänchen shifts in a four-level quantum system. *Int. J. Theor. Phys.* **57**, 2415 (2018).
43. Ruseckas, J. *et al.* Photonic-band-gap properties for two-component slow light. *Phys. Rev. A* **83**, 063811 (2011).
44. Otterbach, J., Ruseckas, J., Unanyan, R. G., Juzeliūnas, G. & Fleischhauer, M. Effective magnetic fields for stationary light. *Phys. Rev. Lett.* **104**, 033903 (2010).
45. Othman, A., Yevick, D. & Al-Amri, M. Generation of three wide frequency bands within a single white-light cavity. *Phys. Rev. A* **97**, 043816 (2018).
46. Huss, A. F., Lammegger, R., Neureiter, C., Korsunsky, E. A. & Windholz, L. Phase correlation of laser waves with arbitrary frequency spacing. *Phys. Rev. Lett.* **93**, 223601 (2004).
47. Phillips, N. B., Gorshkov, A. V. & Novikova, I. Light storage in an optically thick atomic ensemble under conditions of electromagnetically induced transparency and four-wave mixing. *Phys. Rev. A* **83**, 063823 (2011).
48. Scully, M. O. & Zubairy, M. S. *Quantum Optics* (Cambridge University Press, 1997).
49. Born, M. & Wolf, E. *Principles of Optics* 7th edn. (Cambridge University Press, 1999).
50. Liu, N.-H., Zhu, S.-Y., Chen, H. & Wu, X. Superluminal pulse propagation through one-dimensional photonic crystals with a dispersive defect. *Phys. Rev. E* **65**, 046607 (2002).

Acknowledgements

Anas Othman acknowledges financial support from Taibah University. This work is also supported by a grant from King Abdulaziz City for Science and Technology (KACST).

Author contributions

M.A. conceived the idea and supervised the project. A.O. and S.A. carried out the theoretical calculations and analyzed the results. All authors contributed to manuscript writing.

Competing interests

The authors declare no competing interests.

Additional information

Correspondence and requests for materials should be addressed to S.A.

Reprints and permissions information is available at www.nature.com/reprints.

Publisher's note Springer Nature remains neutral with regard to jurisdictional claims in published maps and institutional affiliations.



Open Access This article is licensed under a Creative Commons Attribution 4.0 International License, which permits use, sharing, adaptation, distribution and reproduction in any medium or format, as long as you give appropriate credit to the original author(s) and the source, provide a link to the Creative Commons licence, and indicate if changes were made. The images or other third party material in this article are included in the article's Creative Commons licence, unless indicated otherwise in a credit line to the material. If material is not included in the article's Creative Commons licence and your intended use is not permitted by statutory regulation or exceeds the permitted use, you will need to obtain permission directly from the copyright holder. To view a copy of this licence, visit <http://creativecommons.org/licenses/by/4.0/>.

© The Author(s) 2023